Geometrical and Hemodynamic Variables for Thrombotic Risk Stratification in Kawasaki Disease

Qiong Yao
Children's hospital of Fudan University
Chen Peng
Fudan University
Sheng-zhang Wang
Fudan University
Xi-hong Hu (m18964783309@163.com)
Children's Hospital of Fudan University https://orcid.org/0000-0002-3854-325X

Research Article

Keywords: Hemodynamics, Aneurysm, Kawasaki disease, Computational modeling, Patient-specific simulations,

Posted Date: January 13th, 2022

DOI: https://doi.org/10.21203/rs.3.rs-1248191/v1

Abstract

Objectives

Thrombosis is a major adverse outcome for coronary artery aneurysms (CAA) in Kawasaki disease (KD). We investigated the geometric and hemodynamic abnormalities in patients with CAA and identified the risk factors for thrombosis by computational fluid dynamics (CFD) simulation.

Methods

We retrospectively studied 27 KD patients with 77 CAAs, including 20 CAAs with thrombosis in 12 patients. Patient-specific anatomic models obtained from cardiac magnetic resonance imaging (CMRI) were constructed to perform a CFD simulation. From the simulation results, we produced local hemodynamic parameters comprising of time-averaged wall shear stress (TAWSS), oscillatory shear index (OSI) and relative resident time (RRT). The CAA's maximum diameter (Dmax) and Z-score were measured on CMRI.

Results

Giant CAAs tended to present with more severe hemodynamic abnormalities. Thrombosed CAAs exhibited lower TAWSS (1.551 ± 1.535 vs. 4.235 ± 4.640dynes/cm^2, p = 0.002), higher Dmax (10.905 ± 4.125 vs. 5.791 ± 2.826mm, p = 0.008), Z-score (28.301 ± 13.558 vs. 13.045 ± 8.394, p = 0.002), OSI (0.129 ± 0.132 vs. 0.046 ± 0.080, p = 0.01), and RRT (16.780 ± 11.982s vs. 9.123 ± 11.770s, p = 0.399) than the non-thrombosed group. An ROC analysis for thrombotic risk proved that all of the five parameters had area under the ROC curves (AUC) above 0.7, with Dmax delineating the highest AUC (AUC_{Dmax} = 0.871) and a 90% sensitivity, followed by Z-score ($AUC_{Z-score}$ = 0.849).

Conclusions

It is reasonable to combine the geometric index with hemodynamic information to establish a severity classification for KD cases.

Key Points

1. Giant CAAs and thrombosed CAAs tended to present with more severe hemodynamic abnormalities.
2. ROC analysis for thrombotic risk proved that Dmax and Z-score had the highest AUC than the hemodynamic parameters.
3. Combining the geometric index with hemodynamic information can help to establish a severity classification for KD cases.

1. Introduction

Kawasaki disease (KD), also called mucocutaneous lymph node syndrome, is a systemic median vasculitis with a predominance for coronary arteries. KD is the leading cause of acquired heart disease in children. Coronary artery aneurysm (CAA) is the most common complication of KD, of which the incidence has been reduced greatly from 20–25% to 3–5% by administering aspirin and intravenous immunoglobulin (IVIG) [1, 2]. The American Heart Association (AHA) stated in a scientific statement that KD cases with associated CAAs were classified as at high risk of cardiac events [3]. CAAs may resolve spontaneously in 60% of cases during the subacute and chronic phase, whereas the possibility of thrombosis is the most concerning risk, which can result in myocardial infarction, ischemia-related arrythmias or sudden death. Therapeutic options for CAA in the chronic phase essentially include antiplatelet and anticoagulation therapy. The risk factors for thrombosis have not been totally clarified and the current recommendation of combining antiplatelet and anticoagulant therapy for CAAs at high risk for cardiovascular events is based mainly on the size of CAA: that is, CAAs with a maximum diameter (Dmax) $\geq$ 8 mm or Z-score $\geq$ 10 [4].

Several research articles have suggested that hemodynamic changes in KD patients with CAAs also play a crucial role in the pathogenesis of thrombosis [5–8]. Dilation of the vascular lumen induces a local flow disturbance which results in injury of the endothelium, accelerated platelet aggregation and hypercoagulation. Computational fluid dynamics (CFD) technique can provide multiple hemodynamic parameters including wall shear stress (WSS), relative resident time (RRT), and oscillatory shear index (OSI), which are almost impossible to obtain from usual imaging modalities [9]. The value of CFD in the study of KD has been proven in recent papers, but all the previous research projects were limited by small sample sizes (no more than 10 cases) [6–8]. In the present study, we applied patient-specific CFD in 27 patients with CAAs. We aimed to select variables with high sensitivity and specificity for thrombosis risk stratification.

2. Methods

2.1. Patient population

From May 2016 to February 2019, we enrolled 27 KD patients with CAAs admitted to our medical center. This study was approved by the hospital's Institutional Review Board and written parental consents were obtained. All the data were processed according to the relevant guidelines. A brief clinical history was collected for all the patients, including sex, age, onset of KD, clinical symptoms, treatment, and prognosis. All the patients received echocardiography as first screening exam and were recommended to have cardiac magnetic resonance Imaging (CMRI) when the CAAs were identified. The size of CAA was categorized principally according to Z-score: small (2.5 $\leq$ Z-score < 5), medium (5 $\leq$ Z-score < 10) and giant (Z-score $\geq$ 10 or Dmax $\geq$ 8mm) [4]. The thrombi inside the CAAs were also documented on CMRI images. After CMRI, all the patients had digital subtraction angiography (DSA) to identify the existence and location of CAAs and thrombosis. CMRI and DSA was conducted within 3 days after the

echocardiograms. The disease phases were defined as follows: acute, day 1~14; subacute, day 15~42; and chronic, after day 43. Day 1 was defined as the first day of presenting clinical signs [10].

2.2. CMRI technique

CMRI was performed using a Siemens 1.5T MRI scanner (Siemens Medical Solutions, Erlangen, Germany). The entire protocol included an ECG-gated steady-state free precession (SSFP) sequence with T2 preparation to suppress the myocardium and fat tissues after a bolus of gadobutrol (0.1-0.2 mmol/kg) at a rate of 1-2 ml/s through intravenous line. A 3D volume of axial images including the whole heart was adapted for simulation [11]. Two-dimensional (2D) steady-state free precession segmented cine images in short axial and longitudinal plans with full coverage of the left and right ventricles were acquired for functional assessment. To assess fibrosis, late gadolinium enhancement imaging was conducted by an inversion recovery turbo fast low-angle shot sequence. Imaging was carried out under oral sedation, if necessary.

2.3. 3D anatomical modeling

Patient-specific modeling and a finite element mesh were established using the SimVascular 2018 (Stanford University, USA) to create a patient specific model and the main process included import medical image data, create path, segmentations and 3D geometry model. After importing the created model into ICEM CFD (ANSYS, Inc. USA), the model was used to generate tetrahedral grids and set boundary layers. We also tested grid dependence, when the grid size was less than 0.2cm, the maximum velocity of the outlet of aorta tended to converge. Taking all model considerations into account, the final girds generated were about 150,000 and element numbers 730,000.

The included arteries were the right coronary artery (RCA), the left coronary artery (LCA), the left anterior descending artery (LAD), the left circumflex artery (CCX), as well as the ascending aortic arch.

2.4. Simulation methods

Blood flow simulations were conducted with an Ansys CFX 18.0 solver. Blood was assumed as a Newtonian fluid with a density of 1.06 g/ml, dynamic viscosity of 0.035 dynes/cm·s, and the vessel wall was assumed to be rigid. We used the velocity-time curve of aorta from echocardiogram to set inlet parameter. The LCA, RCA, LAD and CCX were set as flow boundary conditions according to the cross-sectional area of each branch, and the pressure of aorta's outlet was measured by DSA as it was considered as the golden standard. The outlet flow used was the time-average flow and remained the same value throughout the cardiac cycle. The main method was to calculate the total flow according to the inlet velocity, and consider that the total flow of all coronary arteries accounted for 6% of the inlet flow, and then distribute the flow according to the ratio of the outlet cross section area of each coronary artery. We could not measure the time-dependent flow waveform yet. Simulations were operated for 4 cardiac cycles, after which the cycle-to-cycle pressure variations were determined as less than 0.1%. The required simulation time for each model was approximately 20 hours.

2.5. Hemodynamic and geometric variables

Simulated pressure and velocity fields were calculated and hemodynamic variables including time-averaged wall shear stress (TAWSS), OSI and RRT were computed. RRT is the average time a parcel of fluid spends in a specific region based on the pre-computed velocity field. It is a measure of flow stagnation, which contributes to the form of thrombus. How to calculate it is shown in the formula below [12]:

$$TAWSS = \frac{1}{T}\int_0^T \left|wss_i\right| \mathrm{d}t$$

$$OSI = \frac{1}{2}\left\{1 - \frac{\left|\int_0^T wss_i \mathrm{d}t\right|}{\int_0^T \left|wss_i\right| \mathrm{d}t}\right\}$$

$$RRT = \frac{1}{(1-2\times OSI)\times WSS} = \frac{1}{\frac{1}{T}\left|\int_0^T wss_i \mathrm{d}t\right|}$$

Wss_i is the wall shear stress of each grid, and T is the length of a cardiac cycle.

TAWSS, OSI and RRT were temporally averaged over a single cardiac cycle and spatially averaged over each CAA's surface. In addition to hemodynamic variables, we assessed anatomical variables from CMRI, such as location, Dmax and Z-score.

2.6. Statistical analysis

Continuous parameters were presented as mean ± standard deviation and inter-quartile range (IQR). Categorized data were expressed as numbers and percentages. Correlations between hemodynamic and geometric data were evaluated using the Pearson's linear correlation coefficient. We used the unpaired Student's t-test and one-way ANOVA to compare anatomical and hemodynamic variables in the different CAA subgroups. The best cutoff values were obtained from receiver operating characteristic (ROC) curves. SPSS version 26 (IBM SPSS Statistics 26, Armonk, NY, USA) was utilized and p values < 0.05 were considered to have statistically significant difference.

3. Results

Patient demographics and clinical data were summarized and illustrated in Tab. 1. All the patients presented relative symptoms like fever, rash and cervical lymphadenopathy at the onset of the disease. All the patients received aspirin and IVIG in the acute stage, and were treated by the combination of antiplatelet (usually aspirin) and anticoagulation (usually warfarin) when giant CAAs or thrombosis were found by echocardiography or CMRI. The dose of anticoagulation was adjusted to the PT-INR target range of 2.0–2.5.

Table 1
Demographic information of KD patients and anatomical features of CAAs

Sex	
male	20
female	7
Age of onset (month, IQR)	53.58 ± 43.05 (14.75-88.50)
Age of exam (month, IQR)	102.46 ± 56.40 (64.25-151.00)
Follow-up period (month, IQR)	48.88 ± 44.48 (4.75-86.25)
Location of CAAs	
RCA	39/77 (50.65%)
LCA/LAD	30/77 (38.96%)
LAD/CCX	8/77 (10.39%)
Group of CAAs	
Small	13 (16.88%)
median	39 (50.65%)
giant	25 (32.47%)
Z-score of CAAs	
small	3.308 ± 0.309
median	5.408 ± 1.098
giant	11.772 ± 3.331
Thrombosed	20/77 (25.97%)
Non-thrombosed	57/77 (74.03%)

KD = Kawasaki disease; CAA = coronary artery aneurysms; IQR = inter-quartile range; RCA = right coronary artery; LCA = left coronary artery; LAD = left anterior descending; CCX = circumflex coronary artery;

3.1 Anatomical features of CAAs

A total of 27 patient-specific models were constructed and 77 CAAs were analyzed. We outlined the anatomical features of all the 77 CAAs in Tab.1. The findings of DSA were basically consistent with CMRI. Overall, 39 CAAs occurred in the RCA; 30 were formed at the LCA branching site extending to the LAD; 8 developed at the branching site of the LAD and CCX. In some cases, multiple aneurysms existed in a single branch, mainly the RCA. 2 cases exhibited dilation along the whole RCA.

All the CAAs were classified into three groups based on the Z-score (See Tab.1). Regarding the 25 giant CAAs, 9 occurred at the LCA/LAD branching site, 1 at the LAD/CCX region, while the remaining 15 CAAs were located in the RCA. Moreover, the occurrence of the giant CAAs in the RCA was as follows; 6 were in the proximal segment, 5 in the middle segment, 2 in the remote segment, and 2 within the whole dilated RCA.

3.2 Hemodynamic variables in CAAs

Figure 1 displays the distribution of hemodynamic variables in some patients with CAAs. In coronary arteries free of aneurysms, the hemodynamic variables were in the normal range. In the dilated RCA, the disturbance was more obvious in the proximal region with abnormal hemodynamics along the dilated artery (Fig. 1A). The distribution of TAWSS, OSI and RRT were uneven, especially in the giant CAAs (Fig. 1B). As listed in Tab. 2, CAAs with a larger diameter had lower TAWSS, along with higher OSI and longer RRT.

Table 2
Comparison of hemodynamic quantities in different group of CAAs

	Small	**Median**	**Giant**	**F**	***p***
TAWSS (dynes/cm^2)	6.232 ± 4.921	4.152 ± 4.533	1.178 ± 1.248	8.287	0.001
OSI	0.017 ± 0.040	0.040 ± 0.066	0.137 ± 0.133	11.273	0.000
RRT (s)	3.090 ± 3.564	7.669 ± 7.852	20.654 ± 14.837	17.007	0.000

CAA = coronary artery aneurysms; TAWSS = time-averaged wall shear stress; OSI = oscillatory shear index; RRT = relative resident time;

3.3 Geometrical and hemodynamic variables for thrombotic risk stratification

We compared geometric and hemodynamic variables in the thrombosed and non-thrombosed CAAs. All 20 thrombosed CAAs were found in 12 KD patients. For the 12 patients with 20 thrombosed CAAs, 4 cases had IVIG resistant who intended to present more severe inflammatory response and more severe coronary artery impairments. In the 20 thrombosed CAAs, 8 aneurysms occurred at the LCA/LAD branching site; 1 at the LAD/CCX region, and 11 in the RCA. 1 case presented long segmental thrombosis in the mid and remote segment of RCA (Fig. 1A, circle). 1 case had CAAs in the RCA and LAD/CCX, with thrombi in the RCA (Fig. 1C, circle); 1 case developed thrombosis in the distal aneurysm within the RCA rather than proximal (Fig. 1D, circle). Out of all the thrombosed CAAs, 4 were of median size and 16 were of giant size. In median and giant CAAs, the incidence of thrombosis was 10.26% and 64%, relatively. In contrast, no thrombosis was detected in small CAAs.

Pearson correlation coefficients indicated a median correlation between hemodynamic (TAWSS, OSI and RRT) and geometrical variables (Dmax, Z-score) portrayed in Fig. 2.

Quantitative analysis revealed significant discrepancies between the thrombosed and non-thrombosed groups (Fig. 3). Local Dmax (10.905 ± 4.125 vs. 5.791 ± 2.826mm, p = 0.008) and Z-score (28.301 ± 13.558 vs. 13.045 ± 8.394, p = 0.002) in the thrombosed group were considerably higher compared to the non-thrombosed group. With OSI (0.129 ± 0.132 vs. 0.046 ± 0.080, p = 0.010) and RRT (16.780 ± 11.982s vs. 9.123 ± 11.770s, p = 0.399), although the statistics difference for RRT was not significant. The local TAWSS (1.551 ± 1.535 vs. 4.235 ± 4.640dynes/cm^2, p = 0.002) was significantly lower in thrombosed CAAs.

Next, an ROC analysis was conducted based on the geometric and hemodynamic variables, then the associated cutoff value, sensitivities and specificities were presented in Fig. 3. All of the five parameters had area under curves (AUC) larger than 0.7, demonstrating their ability for thrombosis risk stratification. Dmax had the highest AUC (AUC_{Dmax} = 0.871) with 90% sensitivity, followed by Z-score ($AUC_{Z-score}$ = 0.849). OSI (sensitivity = 0.8) and RRT (sensitivity = 0.8) displayed an adequate sensitivity while TAWSS provided a favourable specificity (specificity = 0.8).

4. Discussion

KD is an idiopathic type of acute vasculitis mainly occurring in infants and children younger than 5 years old. Some potential etiologies like certain genetic markers, viral pathogens or immune responses have been reported to be related with KD [13, 14]. It is most common in the Asian race compared to the non-Asian population. In Japan, Korea, and China, the incidence varies from 39 to 250 in 100,000 children < 5 years old, which appears to be on the rise [15, 16]. The prevalence is much lower in non-Asian countries: 17-20 per 100 000 children < 5 years old in the USA, 26.2 in Canada, and 8.4-31 in Europe, with boys having a higher incidence than girls [16].

Coronary artery lesions are the main complications of KD, occurring in up to 40% of patients. CAA has a highest incidence of less than 5% following the administration of IVIG [17, 18]. Other complications associated with KD include coronary artery dilation, thrombosis, stenosis and occlusion, leading to myocardial infarction, heart failure and sudden death. CAA usually forms 2 weeks after onset and thrombosis may be caused by injury to the endothelium and platelet activation. In the chronic phase, there is reconstruction of the vessel wall leading to progressive stenosis, thrombosis and occlusion [5, 19]. Compared with atherosclerosis in adults, thrombus formation in KD is much severe. As instructed by the 2017 AHA and 2014 JCS guidelines, KD necessitates long term management till adulthood.

The size of CAA has always been used as a parameter to distinguish CAAs with higher risks for cardiovascular events. JCS and AHA guidelines of triple-therapy (anticoagulation and dual-antiplatelet therapy) are basically based on the CAA's diameter: Diameter ≥8 mm or z-score ≥10 [4, 20]. Cardiac complications have been proven to be more common in giant aneurysms. In a review by Tsuda consisting

of 245 patients with giant CAA, death, myocardial infarction, and surgery occurred in 15 (6%), 57 (23%), and 90 patients (37%), respectively [21]. In another study composed of 1006 patients covering 44 participating institutions, the cardiac events free rate was 100%, 96%, and 79% for small, medium, and large CAAs [22]. Over 50% of CAA regress to normal size within 5 years and the likelihood of regression seems to highly correlate with the original size of the lesion [23, 24]. In agreement with previous studies, we also confirmed the value of the CAA's size. Dmax ≥ 6.850mm and Z-score ≥ 18.753 may be used as predictors of thrombotic risk.

Some specific locations were prone to form large CAAs and thrombosis, including the LCA/LAD branching site and the RCA's proximal segment. Risk was increased when extensive dilation or multiple aneurysms were found in one coronary artery (Fig. 1A, 1B). Distal aneurysms may be more prone to thrombosis than proximal ones, even those with same sizes and similar hemodynamic dates (Fig. 1D).

Hemodynamic variables could also be useful in risk stratification schemes for CAA. In precedent experimental studies, sites exposed to low WSS and high OSI have been demonstrated to be more susceptible to develop intimal thickening and thrombosis [25–27]. Local low WSS induced platelets aggregation close to the vascular wall and promoted clot formation [28]. Endothelial cells would respond to the hemodynamic changes of low WSS and high OSI to modulate intracellular signaling, stimulating structural remodeling, thrombogenesis, inflammation, and atherosclerosis [5, 25]. Dibyendu discovered that aneurysms with thrombosis presented longer RRT (mean 7.8±2.8 vs. 4.0 ± 2.0) and 108% lower WSS compared to aneurysms without thrombosis [29]. Grande studied 10 KD patients with CAAs and depicted that hemodynamic parameters were sensitive to thrombosis [7].

In Fig. 2, we also noticed a large variation in TAWSS, OSI and RRT in CAAs with similar sizes. The correlation was medium between geometric and hemodynamic variables, in accordance with other papers' reports [7].

Regarding those CAAs with more obvious hemodynamic abnormalities, the risk of thrombosis was higher. For example, compared with larger CAA in LCA/LAD, the dilated RCA exhibited longer RRT along the entire artery, inducing extensive thrombosis (Fig. 1A). Another patient had two CAAs of similar dimensions located in the RCA and LCA/LAD junction, however the hemodynamic abnormalities were more severe in the RCA's CAA (lower TAWSS, higher OSI and RRT), coupled with thrombosis (Fig. 1C). In Fig. 1B and Fig. 1D, RCA had 2 CAAs and had more severe decreased TAWSS. Apart from the decreased TAWSS, the larger CAA demonstrated higher OSI and RRT which prompted the formation of thrombi (Fig. 1B). In Fig. 1D, the thrombosed CAA was in the distal segment of RCA, which had lower blood flow velocity and higher RRT. Our results suggested that hemodynamic parameters can be reliable supplements to the aneurysm size for better predicting thrombotic risk.

Nowadays, CFD studies have been coupled with coronary artery disease, including atherosclerosis, coronary artery bypass grafting surgery, and myocardial bridging [30–32]. Vortices, WSS, OSI, and RRT have been identified as key hemodynamic quantities having the potential to be conventionally used in clinical work. Other new parameters like aneurysm shape index, aneurysm spherality, and aneurysm

surface area have also demonstrated the potential to describe the complexity of aneurysm geometry, but only used in single centers and still require further research to support their accuracy [7, 29, 33]. Based on these facts, we adopted the classical parameters for analysis in our research instead of other new indices.

The results of our study differed somewhat from the smaller study by Grande Gutierrez et al [7]. They applied fluid-structure interactions (FSI) in the modeling which was not adapted in our study. FSI is a technique to combine the change of flow field with the mechanical change of blood vascular wall. However, in order to make the results more reliable, it is necessary to know the accurate parameter of blood vascular wall when calculating fluid-solid coupling. At present, these parameters are difficult to obtain in the pediatric population. There are some papers showing that the WSS varies between FSI and rigid-wall models but the difference sometimes is small to affect the result and clinical use [34, 35]. Moreover, FSI takes a long time and considerable computational power to run, so we chose to set the vessels as rigid walls in this study. In the future, with the progress of technology, FSI can be further used for the study of hemodynamics in our institution.

In our research, we employed a 3D SSFP sequence for patient-specific modeling. Compared to CT angiography, CMRI does not involve any dose of radiologic exposure, which is particularly essential for children in development and in need of serial scanning for future follow-up. Furthermore, CMRI can also be used to observe thrombi and intimal hyperplasia of the coronary artery. The AHA and JCS both uphold the use of CMRI for myocardial injury evaluation and observation of the complete coronary tree during the follow-up of KD patients [36].

5. Limitations

Despite the fact that the number of patients included in this study was modest, we could still identify some limitations. First and foremost, being a retrospective study, there was a large variation in patient age, which may affect the patient characteristics and assumptions. Secondly, the images obtained from CMRI have lower image resolution for very young patients, which could potentially affect the accuracy of modelling. These differences may be improved by using the advanced CMRI scanning technique (higher field strength and spatial resolution). Last but not least, the CFD technique still requires a long period of time for model construction and computing. Hopefully, the increasingly efficient computational methods will enhance the process of simulation to ultimately enable their routine clinical use.

6. Conclusion

In our study, we discovered several points about geometrical and hemodynamic variables correlating with clinical outcomes. The LCA/LAD branching site and the RCA's proximal segment were prone to the formation of giant CAAs and subsequent thrombosis. Moreover, giant CAAs tend to have more severe hemodynamic abnormalities and higher risk of thrombosis. Aneurysm size (Dmax and Z-score) has been proved to be reliable to determine the thrombotic risk. As the most frequently used hemodynamic

parameters based on the CFD technique, TAWSS, OSI and RRT could also be implemented to identify patients at high risk for thrombosis. In future clinical practice, it would be reasonable to combine geometric indices with hemodynamic information for severity classification in KD patients.

Abbreviations

KD Kawasaki disease

CAA coronary artery aneurysm

IVIG intravenous immunoglobulin

AHA American Heart Association

Dmax maximum diameter

CFD computational fluid dynamics

TAWSS time average wall shear stress

WSS wall shear stress

RRT relative resident time

OSI oscillatory shear index

DSA digital subtraction angiography

CMRI cardiac magnetic resonance Imaging

SSFP steady-state free precession

RCA right coronary artery

LCA left coronary artery

LAD left anterior descending artery

CCX circumflex artery

IQR inter-quartile range

ROC receiver operating characteristic

AUC area under the receiver operating characteristic curves

FSI fluid-structure interactions

Declarations

1. **Acknowledgements**

Xi-hong Hu and Sheng-zhang Wang contributed equally to the work.

Qiong yao and Chen Peng contributed equally to the work.

2. **Funding**

The authors declare that no funds, grants, or other support were received during the preparation of this manuscript.

3. **Competing Interests**

The authors have no relevant financial or non-financial interests to disclose.

4. **Author Contributions**

All authors contributed to the study conception and design. Material preparation, data collection and analysis were performed by Qiong Yao and Chen Peng. Xi-hong Hu and Sheng-zhang Wang wrote the first draft of the manuscript and all authors commented on previous versions of the manuscript. All authors read and approved the final manuscript.

5. **Ethics approval**

This study was performed in line with the principles of the Declaration of Helsinki. Approval was granted by the Ethics Committee of Children's Hospital of Fudan University.

6. **Consent to participate**

Written informed consent was obtained from the parents.

7. **Consent to publish**

The authors affirm that human research participants provided informed consent for publication of the images in Figure 1.

References

1. Hearn J, McCrindle BW, Mueller B et al (2018) Spatiotemporal clustering of cases of Kawasaki disease and associated coronary artery aneurysms in Canada. Sci Rep 8:17682
2. Kuo HC (2017) Preventing coronary artery lesions in Kawasaki disease. Biomedical Journal 40:141-146

3. Kavey RE, Allada V, Daniels SR et al (2006) Cardiovascular risk reduction in high-risk pediatric patients: a scientific statement from the American Heart Association Expert Panel on Population and Prevention Science; the Councils on Cardiovascular Disease in the Young, Epidemiology and Prevention, Nutrition, Physical Activity and Metabolism, High Blood Pressure Research, Cardiovascular Nursing, and the Kidney in Heart Disease; and the Interdisciplinary Working Group on Quality of Care and Outcomes Research: endorsed by the American Academy of Pediatrics. Circulation 114:2710-2738
4. McCrindle BW, Rowley AH, Newburger JW et al (2017) Diagnosis, Treatment, and Long-Term Management of Kawasaki Disease: A Scientific Statement for Health Professionals From the American Heart Association. Circulation 135
5. 2014) Guidelines for diagnosis and management of cardiovascular sequelae in Kawasaki disease (JCS 2013). Digest version. Circulation Journal 78:2521-2562
6. Kung E, Kahn AM, Burns JC, Marsden A (2014) In Vitro Validation of Patient-Specific Hemodynamic Simulations in Coronary Aneurysms Caused by Kawasaki Disease. Cardiovasc Eng Technol 5:189-201
7. Grande GN, Mathew M, McCrindle BW et al (2019) Hemodynamic variables in aneurysms are associated with thrombotic risk in children with Kawasaki disease. International Journal of Cardiology 281:15-21
8. Sengupta D, Kahn AM, Burns JC, Sankaran S, Shadden SC, Marsden AL (2012) Image-based modeling of hemodynamics in coronary artery aneurysms caused by Kawasaki disease. Biomech Model Mechanobiol 11:915-932
9. Tsuda E, Singhal M (2018) Role of imaging studies in Kawasaki disease. International Journal of Rheumatic Diseases 21:56-63
10. Sanchez AA, Sexson TS, Almeida-Jones ME, Feagin DJ, Altman CA, Pignatelli RH (2019) Comprehensive left ventricular myocardial deformation assessment in children with Kawasaki disease. Congenital Heart Disease 14:1024-1031
11. Albrecht MH, Varga-Szemes A, Schoepf UJ et al (2018) Coronary artery assessment using self-navigated free-breathing radial whole-heart magnetic resonance angiography in patients with congenital heart disease. European Radiology 28:1267-1275
12. J. VS, O. PL, D. KF, G. DG. (0005-07-20). *Relative residence time and oscillatory shear index of non-Newtonian flow models in aorta*2011 10th International Workshop on Biomedical Engineering, 20111-4. doi: 10.1109/IWBE.2011.6079011
13. Onouchi Y (2018) The genetics of Kawasaki disease. International Journal of Rheumatic Diseases 21:26-30
14. Kuo HC, Hsu YW, Wu MS, Chien SC, Liu SF, Chang WC (2016) Intravenous immunoglobulin, pharmacogenomics, and Kawasaki disease. J Microbiol Immunol Infect 49:1-7
15. Jiao F, Jindal AK, Pandiarajan V et al (2017) The emergence of Kawasaki disease in India and China. Glob Cardiol Sci Pract 2017:e201721

16. Uehara R, Belay ED (2012) Epidemiology of Kawasaki disease in Asia, Europe, and the United States. Journal of Epidemiology 22:79-85
17. Kitano N, Takeuchi T, Suenaga T et al (2020) Seasonal variation in epidemiology of Kawasaki disease-related coronary artery abnormalities in Japan, 1999-2017. Journal of Epidemiology
18. Hearn J, McCrindle BW, Mueller B et al (2018) Spatiotemporal clustering of cases of Kawasaki disease and associated coronary artery aneurysms in Canada. Sci Rep 8:17682
19. Denby KJ, Clark DE, Markham LW (2017) Management of Kawasaki disease in adults. Heart 103:1760-1769
20. Newburger JW, Takahashi M, Burns JC (2016) Kawasaki Disease. Journal of the American College of Cardiology 67:1738-1749
21. Tsuda E, Hamaoka K, Suzuki H et al (2014) A survey of the 3-decade outcome for patients with giant aneurysms caused by Kawasaki disease. American Heart Journal 167:249-258
22. Miura M, Kobayashi T, Kaneko T et al (2018) Association of Severity of Coronary Artery Aneurysms in Patients With Kawasaki Disease and Risk of Later Coronary Events. JAMA Pediatrics 172:e180030
23. Friedman KG, Gauvreau K, Hamaoka-Okamoto A et al (2016) Coronary Artery Aneurysms in Kawasaki Disease: Risk Factors for Progressive Disease and Adverse Cardiac Events in the US Population. Journal of the American Heart Association 5
24. Chih WL, Wu PY, Sun LC, Lin MT, Wang JK, Wu MH (2016) Progressive Coronary Dilatation Predicts Worse Outcome in Kawasaki Disease. J Pediatr 171:78-82
25. Zhou J, Li YS, Chien S (2014) Shear stress-initiated signaling and its regulation of endothelial function. Arterioscler Thromb Vasc Biol 34:2191-2198
26. Genuardi L, Chatzizisis YS, Chiastra C et al (2020) Local fluid dynamics in patients with bifurcated coronary lesions undergoing percutaneous coronary interventions. Cardiology Journal
27. Zuin M, Rigatelli G, Vassilev D, Ronco F, Rigatelli A, Roncon L (2020) Computational fluid dynamic-derived wall shear stress of non-significant left main bifurcation disease may predict acute vessel thrombosis at 3-year follow-up. Heart and Vessels 35:297-306
28. Buck A, Groszek JJ, Colvin DC et al (2018) Combined In Silico and In Vitro Approach Predicts Low Wall Shear Stress Regions in a Hemofilter that Correlate with Thrombus Formation In Vivo. Asaio Journal 64:211-217
29. Sengupta D, Kahn AM, Kung E et al (2014) Thrombotic risk stratification using computational modeling in patients with coronary artery aneurysms following Kawasaki disease. Biomechanics and Modeling in Mechanobiology 13:1261-1276
30. Kamangar S, Salman AN, Badruddin IA et al (2019) Effect of stenosis on hemodynamics in left coronary artery based on patient-specific CT scan. Biomed Mater Eng 30:463-473
31. Mao B, Feng Y, Wang W et al (2020) The influence of hemodynamics on graft patency prediction model based on support vector machine. Journal of Biomechanics 98:109426

32. Sharzehee M, Chang Y, Song JP, Han HC (2019) Hemodynamic effects of myocardial bridging in patients with hypertrophic cardiomyopathy. Am J Physiol Heart Circ Physiol 317:H1282-H1291
33. Grande GN, Kahn A, Burns JC, Marsden AL (2017) Computational blood flow simulations in Kawasaki disease patients: Insight into coronary artery aneurysm hemodynamics. Glob Cardiol Sci Pract 2017:e201729
34. Malvè M, García A, Ohayon J, Martínez MA (2012) Unsteady blood flow and mass transfer of a human left coronary artery bifurcation: FSI vs. CFD. International Communications in Heat and Mass Transfer 39:745-751
35. Chandra S, Raut SS, Jana A et al (2013) Fluid-structure interaction modeling of abdominal aortic aneurysms: the impact of patient-specific inflow conditions and fluid/solid coupling. J Biomech Eng 135:81001
36. Dietz SM, Tacke CE, Kuipers IM et al (2015) Cardiovascular imaging in children and adults following Kawasaki disease. Insights Imaging 6:697-705

Figures

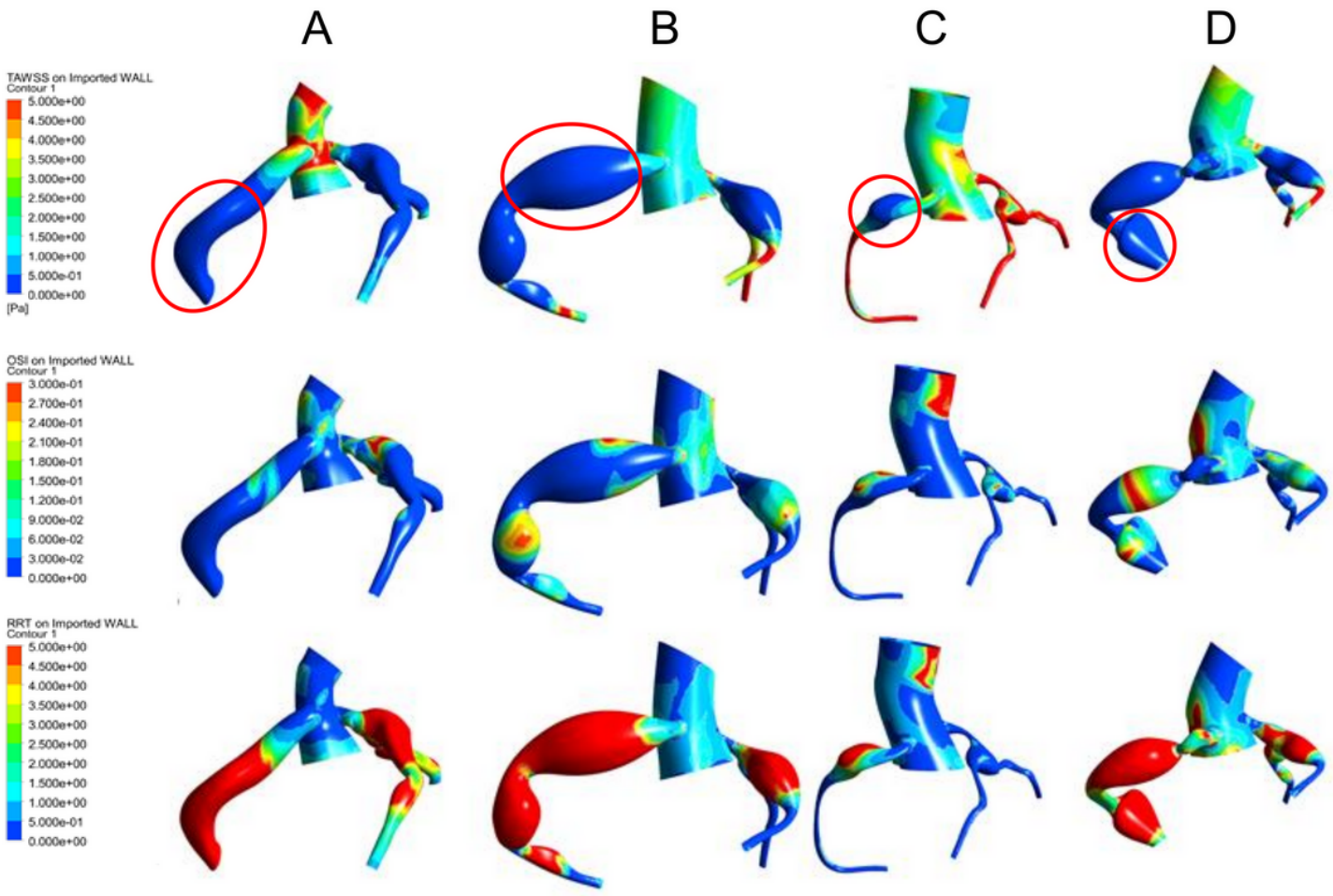

Figure 1

The distribution of hemodynamic variables in 4 patients. A: abnormal hemodynamics along the dilated RCA with extensive thrombi in the mid and remote segment (circle); B: multiple CAAs in the RCA with thrombi in the proximal giant CAA (circle); C: CAAs in the RCA and LAD/CCX, with thrombi in the RCA (circle); D: multiple CAAs in the RCA with thrombosis in the distal CAA, coupled with lower TAWSS, higher OSI and RRT (circle).

CAA = coronary artery aneurysms; RCA = right coronary artery; LCA = left coronary artery; LAD = left anterior descending; CCX = circumflex coronary artery; TAWSS = time-averaged wall shear stress; OSI = oscillatory shear index; RRT = relative resident time;

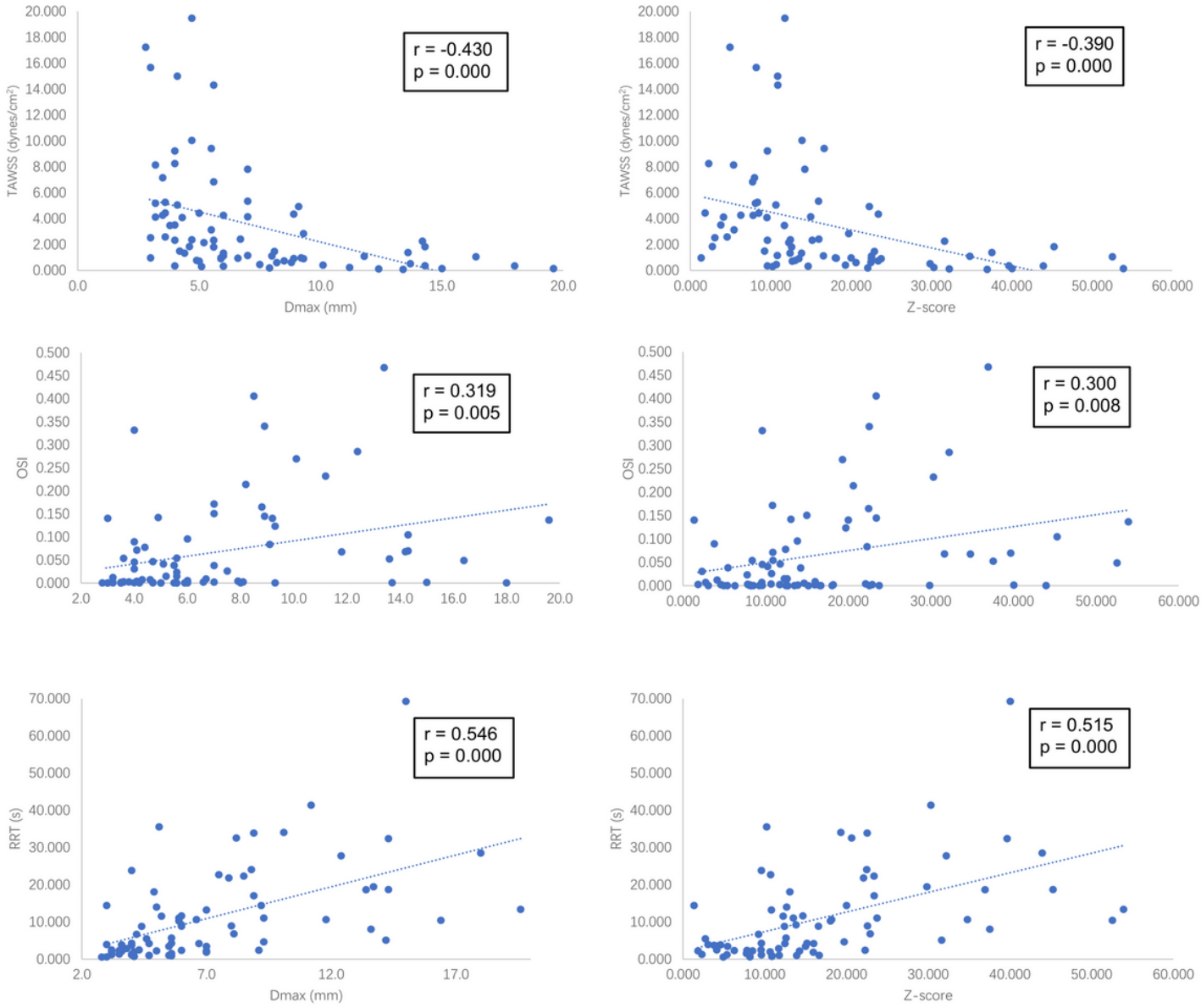

Figure 2

Pearson correlation coefficients indicated a median correlation between hemodynamic (TAWSS, OSI and RRT) and geometrical variables (Dmax, Z-score).

Dmax = maximum diameter; TAWSS = time-averaged wall shear stress; OSI = oscillatory shear index; RRT = relative resident time;

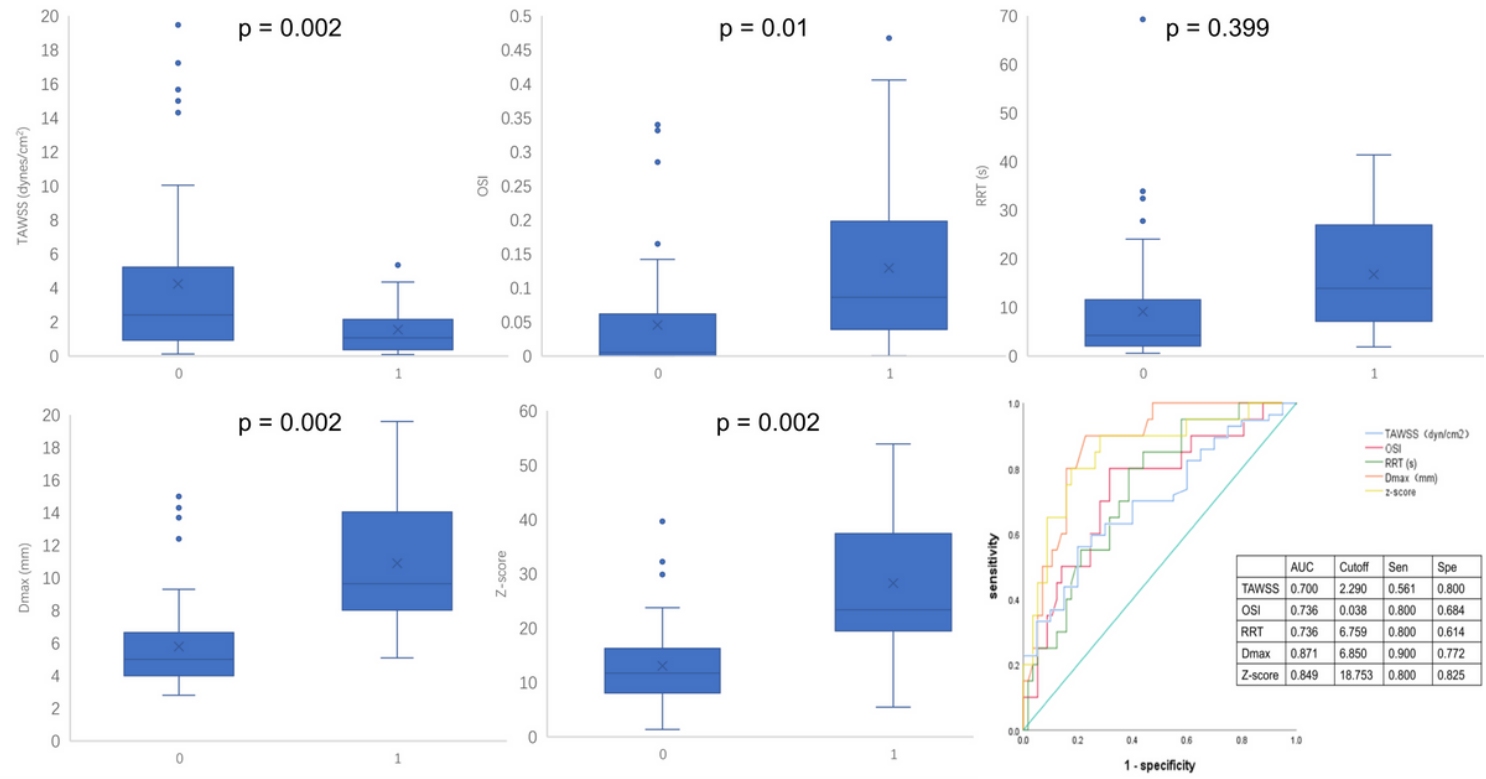

Figure 3

Unpaired Student's t-test revealed significant discrepancies of hemodynamic (TAWSS, OSI and RRT) and geometrical variables (Dmax, Z-score) between thrombosed and non- thrombosed groups. ROC analysis showed that all of the five parameters had AUC larger than 0.7, demonstrating their ability for thrombosis risk stratification.

Dmax = maximum diameter; TAWSS = time-averaged wall shear stress; OSI = oscillatory shear index; RRT = relative resident time; 0 = non-thrombosed group; 1 = thrombosed group; ROC = receiver operating characteristic; AUC = area under the ROC curve; sen = sensitivity; spe = specificity;